Universidad Adolfo Ibáñez

Faculty of Engineering and Sciences

Mechanical and Microstructural Properties of Cement Pastes with Partial OPC Replacement by Copper Slag Flotation Tailings

Author:
Juan Ignacio Rodríguez Valenzuela

Supervisor:
Prof. Federico C. Antico

Committee:
Prof. Paula Rojas
Prof. Danny Guzmán

Thesis submitted in partial fulfillment of the requirements for the degree of Master of Science in Civil Engineering

January 2026

UAI FACULTAD DE INGENIERÍA Y CIENCIAS

Agradecimientos

Llegar a este momento marca el cierre de un proceso largo, exigente y profundamente significativo, que no habría sido posible sin el apoyo de muchas personas que, de distintas maneras, estuvieron presentes a lo largo de este camino académico y personal.

En primer lugar, quiero agradecer a las dos personas más importantes de mi vida: **Juan Rodríguez Donoso** y **Lina Valenzuela Solís**, mis padres. A lo largo de los años he sido testigo de su esfuerzo constante y de jornadas de trabajo exigentes, muchas veces poco valoradas, siempre con el objetivo de sacar adelante a mi hermana y a mí. Su apoyo incondicional, junto con los valores que me han transmitido, han sido una fuente permanente de inspiración y admiración. No imagino aún el día en que pueda decir que he llegado a ser una persona tan íntegra y generosa como ellos, pero sin duda es a lo que aspiro.

Quiero expresar mi más sincero agradecimiento a mi profesor guía, **Prof. Federico C. Antico**, quien no solo me incentivó a continuar mis estudios de magíster, sino que además confió en mí durante todo este proceso. Agradezco especialmente su disposición permanente al diálogo, su respeto por mis limitaciones y su capacidad para ver potencial incluso en momentos complejos. Su apoyo, criterio y guía fueron fundamentales para enfrentar un camino tan desafiante como el desarrollo de esta tesis.

Agradezco también a los miembros de mi comisión evaluadora, **Prof. Paula Rojas** y **Prof. Danny Guzmán**, por su disposición a formar parte de este proceso ayudandome a fortalecer y mejorar la calidad de este trabajo.

Esta investigación se desarrolló en el marco del proyecto **FONDEF**, cuyo apoyo fue fundamental para la ejecución del programa experimental y el desarrollo del estudio. En este contexto, quisiera agradecer especialmente a **Carlos**, estudiante de la Universidad de Atacama, por su colaboración directa en este trabajo y por su participación activa en el proyecto, aportando de manera significativa al desarrollo del manuscrito.

Dado el extenso tiempo dedicado al trabajo experimental, deseo agradecer de manera especial a **Wladimir Vergara**, encargado del laboratorio de materiales, lugar donde comenzó gran parte de este proceso. A pesar de nuestras diferencias en la forma de trabajar, su liderazgo y compromiso hicieron posible llevar a cabo extensas jornadas de laboratorio en condiciones muy diversas: con sol, con lluvia, fines de semana, durante el verano y en períodos de descanso. Su profesionalismo y calidad humana permitieron que cada etapa se completara con éxito y, con el tiempo, ese trabajo compartido dio paso a una amistad que valoro profundamente.

Asimismo, quiero agradecer a mis compañeros de magíster, quienes compartieron tanto las dificultades como las alegrías propias de este proceso. En particular, a **Sander, Tomás, Michela y Simón**, mis compañeros generacionales en la Universidad Adolfo Ibáñez, con quienes compartí innumerables experiencias académicas desde el pregrado hasta estos dos años de magíster. Su compañía, apoyo y amistad hicieron que los momentos de mayor exigencia fueran mucho más llevaderos. De igual forma, agradezco a **Vicho, Manu y Pipe**, quienes se sumaron durante el último año y transformaron la convivencia académica en una experiencia de compañerismo y amistad que valoro sinceramente.

Finalmente, quiero agradecer a mis amigos de la vida, quienes han estado presentes en todas mis facetas y han sabido acompañarme incluso en mis momentos más difíciles. A **Benjamín "el terror de Pulin" Cornejo**, mi amigo más antiguo, con quien incontables caminatas breves terminaron convirtiéndose en largas conversaciones llenas de risas. A mis

queridas amigas de la Universidad Técnica Federico Santa María, **Fran**, ejemplo de lealtad, convicción y fortaleza, y **Carlita**, una amistad nacida por casualidad, siempre dispuesta a decirme las cosas de frente y a estar presente en cada etapa emocional compleja.

Mención especial merece también el grupo de amigos que nació inesperadamente en una clase de educación física de primer año y que con el tiempo se transformó en un pilar fundamental de mi vida. **Nacho, Claudio, Labe, Max, Maxi, Alonso, Nacho y Agustín**, cada uno con su personalidad única, han demostrado que las diferencias no impiden construir una amistad sólida basada en el apoyo mutuo y la presencia constante.

Sin duda, todas estas personas han sido parte fundamental no solo de este trabajo académico, sino también de mi crecimiento personal. Es posible que, al escribir estas líneas, haya omitido mencionar a alguien, pero quiero dejar en claro que cada apoyo, cada conversación y cada gesto han sido profundamente valorados. A todos ustedes, muchas gracias.

Viña del Mar, enero de 2026
Juan Ignacio Rodríguez Valenzuela

Abstract

The growing need to reduce the environmental impact of cement production has intensified interest in alternative supplementary cementitious materials derived from industrial by-products. In this study, copper slag flotation tailings (CSFT) obtained from the reprocessing of copper smelting residues were evaluated as a partial replacement of Ordinary Portland Cement (OPC) in cement pastes.

Six mixtures were prepared by replacing OPC with CSFT at levels of 5–30% by mass, using a constant water-to-binder ratio of 0.30. Mechanical performance was assessed through compressive and flexural strength testing at curing ages up to 180 days. Complementary nondestructive techniques, including ultrasonic pulse velocity and electrical resistivity, were employed to monitor microstructural development, while thermogravimetric analysis (TGA) was used to quantify hydration products associated with C–S–H and portlandite.

Results show that CSFT replacement above 20% leads to reduced early-age mechanical performance of hardened pastes, primarily due to clinker reduction and the low initial reactivity of the CSFT. However, progressive strength recovery was observed from 56 days onward. In particular, mixtures with low CSFT contents (5–10%) approached or matched the OPC mixtures in mechanical–strength by 90–180 days. TGA results revealed that the mass loss associated with C–S–H and chemically bound water increased with curing age and converged across all mixtures at 180 days, whereas portlandite content remained consistently lower with increasing CSFT replacement and did not exhibit recovery at later ages.

These findings indicate that CSFT behaves predominantly as a filler material with possible low intrinsic reactivity, while potentially contributing to delayed secondary hydration processes at extended curing ages. The decoupled evolution of C–S–H formation and portlandite content highlights the importance of extended curing evaluations when assessing low-reactivity cementitious additions. Overall, CSFT shows potential as a sustainable clinker-reducing component in cementitious systems when applied at moderate replacement levels and evaluated beyond standard 28-day performance criteria.

Contents

Introduction

The global cement industry faces increasing pressure to reduce its environmental impact due to the high carbon footprint associated with Ordinary Portland Cement (OPC) production. Cement manufacturing is estimated to contribute approximately 5–10% of global anthropogenic CO_2 emissions, largely driven by clinker production and limestone calcination processes [1, 2]. In Chile, cement demand has increased steadily over recent decades as a result of urban expansion and public infrastructure development, with annual consumption exceeding 5.2 million tonnes in 2023 [3]. In this context, the combination of sustained demand growth and national decarbonization commitments has intensified interest in low-carbon cementitious systems capable of reducing clinker content without compromising long-term performance.

Supplementary cementitious materials (SCMs) have long been recognized as effective partial replacements for OPC, contributing to improved durability and reduced CO_2 emissions associated with concrete production [2, 4]. Traditionally used SCMs include fly ash, ground granulated blast furnace slag, and silica fume, which exhibit pozzolanic or latent hydraulic behavior and can enhance mechanical performance and microstructural refinement [4, 5]. However, the availability of certain conventional SCMs—particularly fly ash—has declined significantly in regions transitioning away from coal-based energy generation [2, 5]. This limitation has motivated the search for alternative, locally available SCMs capable of supporting cement decarbonization strategies.

Mining by-products have emerged as promising candidates for use as supplementary cementitious materials, particularly due to their chemical similarity to traditional pozzolans and their large-scale availability. Chile generates over 500 million tonnes of mining tailings annually [3], highlighting the potential of these materials as sustainable cementitious constituents. Among these residues, copper slag and its derivatives have received increasing attention. Copper smelting produces a vitrified slag rich in SiO_2, Fe_2O_3, and Al_2O_3, phases that may participate in hydration reactions when appropriately processed [6, 7]. Several studies report that treated copper slag can act as a supplementary cementitious material, with optimal replacement levels typically ranging between 15 and 20% [6, 8]. Mechanical or thermal activation has been shown to enhance reactivity by increasing amorphous content or reducing particle size [7].

Beyond mechanical performance, the use of mine tailings in cementitious systems has raised environmental and health concerns related to the potential leaching of trace elements and heavy metals into soil and groundwater [9]. As a result, recent literature emphasizes that the evaluation of tailings-based construction materials should not rely solely on mechanical characterization, but also consider toxicity-related assessments such as pH, electrical conductivity, heavy metal content, and standardized leaching tests (e.g., U.S. EPA Method 1311, TCLP) [10]. Recent sustainability-oriented reviews further identify environmental compliance and long-term leaching behavior as key bottlenecks for the large-scale adoption of tailings-derived SCMs, highlighting the need for clearer regulatory frameworks and extended assessment protocols [11].

Recent technological advances in the beneficiation of copper smelting residues—particularly grinding, flotation, and classification—have led to the production of copper slag flotation tailings (CSFT), a fine material with particle sizes typically below 60–75 μm. Beyond chemical composition, particle size distribution plays a critical role in governing the performance of SCM-containing systems, as fineness directly influences particle packing, dispersion, and

physical interactions with the cement matrix [12, 13]. Finer SCMs may act predominantly as fillers at early ages, enhancing packing density and reducing effective porosity, even in the absence of significant chemical reactivity [14].

In this context, the reduction of coarse particles and the narrowing of the particle size distribution—often quantified through parameters such as D50 and D90—are particularly relevant. Materials with lower D90 values exhibit reduced coarse tails, which may improve homogeneity and promote more effective physical interaction between SCM particles and OPC grains, facilitating nucleation and continued hydration [6, 13]. These effects are especially pronounced in systems where SCMs exhibit limited intrinsic reactivity, as physical mechanisms dominate early-age behavior.

At the same time, the predominantly crystalline nature observed in the CSFT by XRD suggests limited intrinsic reactivity, which raises the possibility of delayed or slow pozzolanic reactions developing at later curing stages, as reported for low-calcium fly ash and other moderately reactive SCMs [4, 15, 16]. Suraneni and Weiss emphasized that SCM reactivity should not be assessed solely through calcium hydroxide consumption, but also through the evolution of chemically bound water, as these parameters help distinguish inert fillers from slowly reacting materials [15].

Studies on copper slag–based SCMs report contrasting results depending on chemical composition, treatment history, particle size, and curing conditions. Some authors observed calcium hydroxide consumption and long-term strength gains associated with secondary C–S–H formation [6, 8], whereas others described copper slag residues primarily as filler materials with limited early-age reactivity [7]. Similar behavior has been reported for other silica-rich SCMs, such as rice husk ash or finely ground minerals, which tend to contribute predominantly through physical effects at early ages, with pozzolanic activity emerging only after extended curing [13, 14, 17, 18].

The role of the water-to-binder ratio is also critical when assessing the contribution of SCMs and filler materials. Low water-to-binder ratios are known to amplify physical effects such as particle packing, dilution, and nucleation by reducing capillary porosity and increasing the solid volume fraction [12, 13]. Under such conditions, differences in particle size distribution and fineness become more influential, allowing a clearer evaluation of the physical and potential chemical contributions of low-reactivity materials. Accordingly, low w/b systems are particularly suitable for assessing SCMs whose behavior is expected to be governed primarily by filler-related mechanisms at early ages [14].

Despite these advances, the literature addressing *flotation-derived* copper slag tailings remains limited. Most existing studies focus on untreated furnace slags [6–8], leaving a knowledge gap regarding the hydration behavior, microstructural evolution, and mechanical response of CSFT. It remains unclear whether CSFT should be classified as an inert filler, a pozzolanic material, or a hybrid system exhibiting delayed reactivity. Given the large-scale availability of CSFT in Chile and its potential to contribute to clinker reduction, a systematic evaluation of its role in cement hydration is required.

The present study addresses this gap by investigating cement pastes in which OPC is partially replaced (5–30%) by CSFT. A comprehensive experimental program is employed, including mechanical testing (compressive and flexural strength), nondestructive techniques (ultrasonic pulse velocity and electrical resistivity), and thermogravimetric analysis (TGA) to quantify mass losses associated with C–S–H, calcium hydroxide, and carbonate phases. This

multi-technique approach enables the distinction between physical filler effects and delayed chemical contributions, providing insight into the mechanisms governing both early- and late-age behavior of CSFT-modified systems.

Based on the characteristics reported for copper slag–derived materials and other low-reactivity SCMs, CSFT is expected to differ from conventional highly reactive pozzolans and to exhibit behavior dominated by physical filler effects at early ages, with potential contributions developing at extended curing times. In such systems, reductions in early-age mechanical performance are commonly associated with clinker dilution, whereas progressive strength development at later ages is linked to continued hydration and, in some cases, slow secondary reactions. These considerations align with recent frameworks questioning the adequacy of 28-day strength as the sole performance benchmark for low-reactivity SCMs [18], and motivate the evaluation of CSFT as a potential clinker-reducing material while preserving long-term mechanical performance.

Materials and Methods

2.1 Raw materials

OPC (Type I), supplied by Polpaico Solutions, Chile, was used as the cementitious material for the primary binder. The cement properties were provided by an official testing report issued by IDIEM (Investigación, Desarrollo e Innovación de Estructuras y Materiales), Universidad de Chile [19]. Table 2.1.1 summarizes the main physical and mechanical properties of the OPC used in this study, as reported by IDIEM[19]. CSFT used in this study were sourced from the Manuel Antonio Matta plant, operated by the Empresa Nacional de Minería (ENAMI) in Chile. At this facility, copper smelting slags are reprocessed to recover residual copper. The process involves a comminution stage (crushing and grinding) followed by a slag flotation circuit, from which the CSFT is generated as a by-product. A 10-ton pulp sample was collected from the courier sampling point of the industrial slag flotation circuit. This bulk sample was transported to the facilities of the IDICTEC (Instituto de Investigación, Desarrollo e Innovación Tecnológica de la Universidad de Atacama) for processing. The pulp underwent a drying process involving solar drying and decantation of clear water, which yielded 3.5 tons of dry CSFT. Subsequently, this material was homogenized using the coning and quartering method to ensure uniformity. The homogenized CSFT was then packaged into approximately 135 representative samples of 25 kg each. These samples were delivered to the Department of Metallurgy at the Universidad de Atacama and constituted the CSFT raw material for this research.

Table 2.1.1. Test results for the OPC used in this study, according to the official IDIEM report[19].

Test performed	**Unit**	**Sample**	**Requirements according to NCh148**
Specific gravity	g/ml	3.18	$\geq$ 3.00 g/ml
Specific surface area	cm^2/g	3150	Not applicable
Standard consistency water	%	26.25	Not applicable
Setting time – Initial	h:min	03:00	$\geq$ 00:45 h:min
Setting time – Final	h:min	04:00	$\leq$ 10:00 h:min
Autoclave expansion	%	0.02	$\leq$ 1.00 %
Mechanical strength – Flexural (7 days)	kgf/cm^2	64	$\geq$ 45 kgf/cm^2
Mechanical strength – Flexural (28 days)	kgf/cm^2	90	$\geq$ 55 kgf/cm^2
Mechanical strength – Compressive (7 days)	kgf/cm^2	431	$\geq$ 250 kgf/cm^2
Mechanical strength – Compressive (28 days)	kgf/cm^2	632	$\geq$ 350 kgf/cm^2
Loss on ignition	%	1.1	$\leq$ 3.0 %
SO_3 content	%	2.67	$\leq$ 4.00 %
Insoluble residue	%	0.5	$\leq$ 1.5 %
MgO content	%	1.5	$\leq$ 5.0 %
Mn_2O_3 content	%	–	Not applicable

In addition to its physical characterization, the environmental suitability of the CSFT was assessed through toxicity-related leaching tests. The Toxicity Characteristic Leaching Procedure (TCLP) was performed in accordance with NCh 2754 (EPA Method 1311)[20, 21] on representative CSFT samples collected at different stages of the hydrocyclone classification process, including two feed samples as well as overflow and underflow fractions. The concentrations of regulated elements in the leachates were compared with the maximum permissible limits for hazardous waste classification. Results showed that all analyzed elements were either well below the corresponding regulatory thresholds or below the analytical quantification limits, indicating that the CSFT used in this study does not exhibit hazardous leaching behavior under TCLP conditions.

The crystalline phases of CSFT were identified by X-ray diffraction (XRD). The analysis was performed using a Shimadzu XRD-6100 diffractometer with Cu Kα radiation. The resulting diffraction data were processed using X'Pert HighScore Plus software. Phase identification was guided by the elemental composition obtained from SEM–EDS, and diffraction peaks were matched against the Powder Diffraction File (PDF) database, with each phase verified on a peak-by-peak basis. As shown in the XRD pattern in Figure 2.1, the main crystalline phases identified in CSFT were fayalite, magnetite, quartz, and diopside.

Table 2.1.2. TCLP leaching results for CSFT samples at different stages of the hydrocyclone classification process and corresponding regulatory limits.

Sample	**Ba** (mg/L)	**Pb** (mg/L)	**As** (mg/L)	**Cd** (mg/L)	**Cr** (mg/L)	**Hg** (mg/L)	**Ag** (mg/L)	**Se** (mg/L)
Feed 1	0.71	0.24	<0.097	<0.031	<0.142	<0.019	<0.141	<0.203
Feed 2	0.74	0.25	<0.097	<0.031	<0.142	<0.019	<0.141	<0.203
Overflow	0.145	0.145	<0.097	<0.031	<0.142	<0.019	<0.141	<0.203
Underflow	0.190	0.190	<0.097	<0.031	<0.142	<0.019	<0.141	<0.203
Regulatory limit	100	5.0	5.0	1.0	5.0	0.2	5.0	1.0

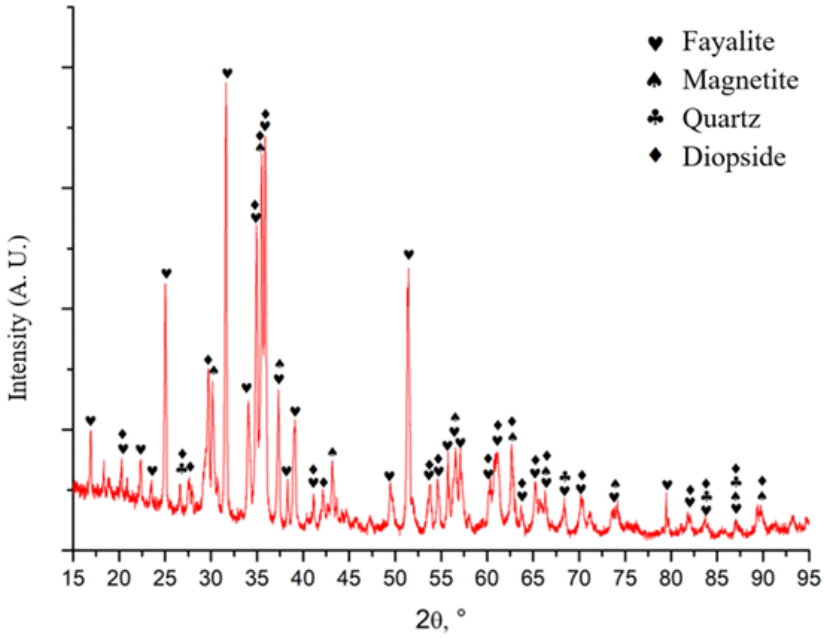

Figure 2.1. X-ray diffraction (XRD) pattern of copper slag flotation tailings (CSFT). The main crystalline phases identified are fayalite, magnetite, quartz, and diopside. Symbols indicate the reference peak positions from the Powder Diffraction File (PDF) database used for phase identification.

2.2 Processing of CSFT

After collection, the copper slag flotation tailings (CSFT) were subjected to a hydraulic classification process developed at the Universidad de Atacama using a laboratory-scale hydrocyclone pilot plant. Hydrocyclone classification is a well-established particle separation technology widely applied in mineral processing and waste valorization to reduce particle size and remove coarse and heterogeneous fractions [22, 23]. In this study, the fine fraction recovered from the overflow stream was selected and used for the preparation of cement pastes incorporating CSFT as partial OPC replacement.

Hydrocyclones operate by generating a high-intensity centrifugal field that separates particles according to their size, density, and hydrodynamic behavior. While the process is commonly employed to enrich fine fractions, it is also well documented that the separation is not purely sharp and that the overflow fraction may retain a certain proportion of coarser particles, leading to a broader particle size distribution [24–26]. This characteristic reflects the complex and partially non-deterministic nature of the flow field within hydrocyclones and is inherent to their operation.

As a result of the classification process, the CSFT exhibited a significantly finer particle profile compared to the OPC reference, as evidenced by the particle size distribution curves

presented in Figure 2.3. The classified CSFT showed a D50 of approximately 11.5 µm and a D90 of about 52 µm, whereas OPC exhibited a D50 of approximately 26.1 µm and a D90 of about 73.2 µm. These values confirm an effective reduction in characteristic particle sizes and the removal of a substantial portion of the coarse fraction. At the same time, the presence of a residual coarse tail in the classified CSFT distribution indicates that particles of varying sizes remain after classification, resulting in a wider distribution span, a feature commonly reported for hydrocyclone overflow products [24, 25].

Scanning electron microscopy (SEM) observations (Figure 2.2) qualitatively support the laser diffraction results. OPC particles exhibit a comparatively coarser morphology, consistent with their higher D90 value, whereas the classified CSFT shows a predominance of finer and more angular particles, together with occasional larger grains. This combination of fine and coarser particles may enhance physical interactions between OPC and CSFT through improved particle packing and contact during hydration, as reported in previous studies addressing the influence of particle size and filler effects in cementitious systems [6, 7].

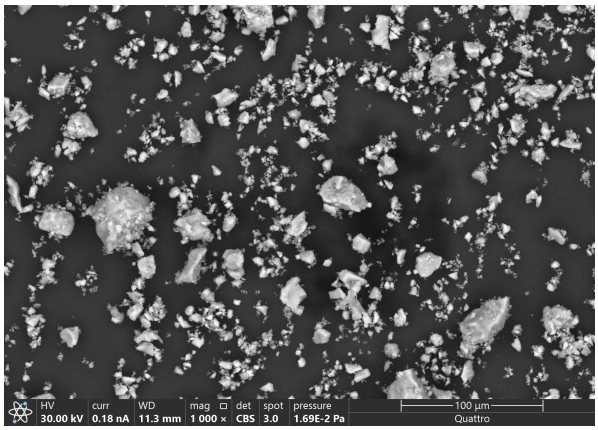

(a) SEM micrograph of OPC powder.

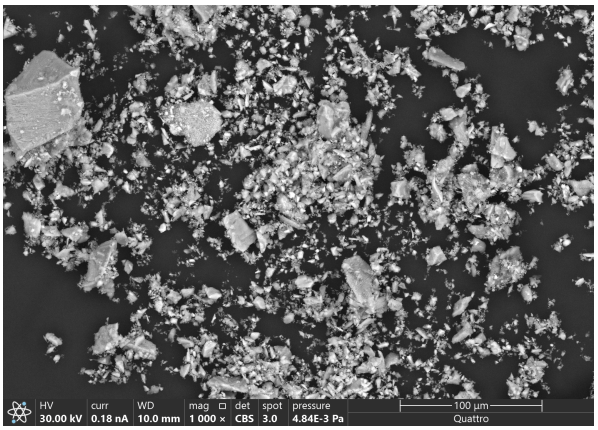

(b) SEM micrograph of CSFT powder.

Figure 2.2. SEM micrographs of (a) OPC and (b) hydrocyclone-classified CSFT powders. OPC particles exhibit a comparatively coarser morphology, consistent with their higher D90 value, whereas the classified CSFT shows a predominance of finer and more angular particles. These observations qualitatively support the particle size distribution results and highlight the morphological differences between both powders.

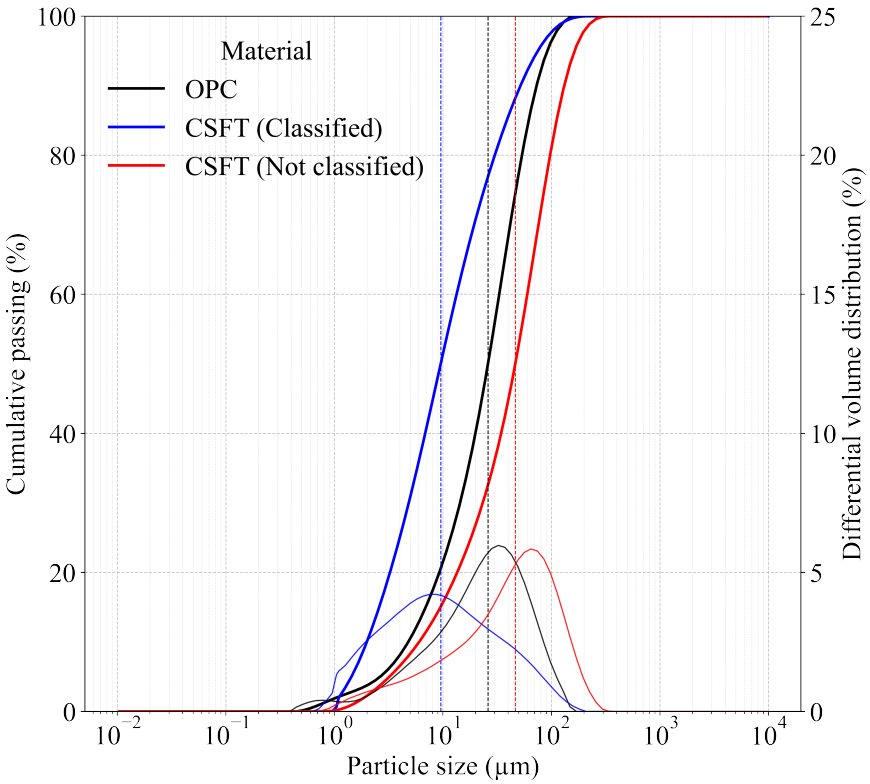

Figure 2.3. Particle size distributions obtained by laser diffraction for OPC (black curves), raw flotation tailings CSFT (red curves), and hydrocyclone-classified CSFT (HCSFT, blue curves). The cumulative passing curves are shown on the left axis, while the differential volume distributions are presented on the right axis. Vertical dashed lines of matching color indicate the corresponding median particle size (D50) for each material. OPC exhibits an intermediate particle size distribution (D50 $\approx$ 26.1 µm; D90 $\approx$ 73.2 µm), whereas raw CSFT shows a coarser profile with a rightward shift of the cumulative curve. In contrast, the hydrocyclone-classified CSFT presents a markedly finer distribution (D50 $\approx$ 11.5 µm; D90 $\approx$ 52 µm), reflected by the leftward displacement of the cumulative curve and its characteristic diameters. The differential volume distributions further indicate a broader particle size span for the classified CSFT, highlighting the presence of residual coarse particles inherent to the hydrocyclone separation process. Measurements were performed using a Malvern Mastersizer 2000 laser diffraction analyzer.

2.3 Mixture design, sample preparation, and curing conditions

2.3.1 Reference CSFT mixtures

Six cement paste mixtures were prepared by partially replacing Ordinary Portland Cement (OPC) with CSFT at replacement levels of 0%, 5%, 10%, 15%, 20%, and 30% by mass of binder, designated as OPC, CSFT-05, CSFT-10, CSFT-15, CSFT-20, and CSFT-30, respectively. All mixtures were produced using a constant water-to-binder ratio (w/b) of 0.30. This relatively low w/b ratio was intentionally selected to enhance the physical contribution of supplementary cementitious materials and fine fillers. At low water contents, particle packing, fineness, and dispersion effects become more influential, allowing a clearer assessment of dilution and filler-related mechanisms associated with CSFT incorporation. Additionally, preliminary trials confirmed that a w/b of 0.30 provided sufficient workability even at the highest replacement level, while enabling demolding after 24 h.

Mixtures were prepared by first dry-blending the solid constituents to ensure uniform distribution of OPC and CSFT. Water was then added gradually, and mixing was performed using an electric handheld mixer for 2–3 min, followed by manual kneading to eliminate remaining agglomerates and achieve complete paste homogenization.

Fresh pastes were cast into oiled prismatic molds (4 × 4 × 16 cm) in two layers. Each layer was compacted by vibration for approximately 8 s to remove entrapped air. Immediately after casting, molds were covered with a plastic sheet to minimize moisture loss during the first 24 h. Specimens were subsequently demolded, labeled, and cured by immersion in water at 20 ± 2 °C until testing.

Mechanical and durability-related tests were conducted at curing ages of 2, 7, 14, 28, 56, 90, and 180 days. At least three prisms per mixture were allocated for each testing series.

2.3.2 Additional mixtures

Complementary mixtures were prepared to evaluate the influence of thermally treated CSFT and a commercial natural pozzolan (NP). CSFT was thermally treated at 600 °C, 700 °C, and 800 °C for 2 h in a programmable muffle furnace prior to mixing, using a fixed replacement level of 20% and the same procedures described above. For the natural pozzolan series, OPC was partially replaced by 5%, 10%, 15%, and 20% NP supplied by Polpaico Solutions; the 30% replacement level was excluded due to poor mechanical performance observed at higher substitution levels. All additional mixtures were tested following the same experimental protocols as the CSFT-based samples, except that TGA was not performed for these series.

2.4 Experimental methods

2.4.1 Non-destructive tests

Surface electrical resistivity was measured using a Proceq Resipod four-point Wenner probe, in accordance with ASTM C1876 (equivalent to AASHTO TP119)[27]. Measurements

were performed on the three lateral faces of each prism, excluding the casting surface. One reading was taken per face, and the average of the three readings was reported as the representative resistivity value.All measurements were conducted immediately after removing the specimens from the curing water. Prior to testing, excess surface water was gently removed using an absorbent cloth to avoid interference from free moisture.

Ultrasonic pulse velocity (UPV) measurements were performed in accordance with ASTM C597 [28] using 54 kHz transducers. The transmitter and receiver were placed on the 4×4 cm end faces of the prism, allowing direct pulse transmission along the 16 cm length of the specimen. The transit time of the compressional wave was recorded, and the ultrasonic pulse velocity (v) was calculated as:

$$v = \frac{L}{t} \tag{2.4.1}$$

where L is the specimen length (0.16 m) and t is the measured travel time.

Measurements were performed immediately after removing the specimens from the curing water, following gentle removal of surface moisture. Only readings with a device-indicated confidence level of 100% were accepted. Three valid measurements were recorded per specimen, and the mean value was reported.

Dimensional characterization Prior to destructive testing, each specimen was dimensionally characterized. Length was measured at two locations along the prism axis, while height and width were measured at three positions (at one-quarter, one-half, and three-quarters of the length). The measured dimensions were used to calculate flexural and compressive strength according to standard equations, thereby accounting for geometric variability among specimens.

2.4.2 Mechanical and physical tests

Flexural strength was determined using a three-point bending configuration, following the general principles of ASTM C348 [29]. A span length of 100 mm was adopted. Specimens were loaded under displacement control at a constant rate of 0.5 mm/min using a universal testing machine until failure.

Flexural strength (f_{f}) was calculated as:

$$f_{\mathrm{f}} = \frac{3FL}{2bh^2} \tag{2.4.2}$$

where F is the maximum applied load, L is the span length, and b and h are the measured width and height of the specimen, respectively. Three prisms per mixture were tested at each curing age.

Compressive strength After flexural testing, each prism was divided into two halves of approximately $4 \times 4 \times 8$ cm. These halves were tested in compression following the general principles of ASTM C349 [30], using loading platens adapted to the reduced specimen size.

Load was applied under displacement control at a constant rate of 0.5 mm/min, perpendicular to the 4 × 4 cm faces, until failure.

Compressive strength (f_c) was calculated as:

$$f_c = \frac{F}{A} \tag{2.4.3}$$

where F is the maximum applied load and A is the loaded cross-sectional area. Six compression tests were performed per mixture and curing age.

Thermogravimetric analysis (TGA) Additional paste samples were prepared using the same mixture proportions as the rest of the experimental program and cast into small cylindrical molds to produce pellets of approximately 0.4 cm^3. Eight pellets per mixture were fabricated to cover the target curing ages (2, 7, 28, 56, 90, and 180 days). After 24 h under plastic cover, the pellets were demolded and cured by immersion in distilled water at a temperature of 20 °C.

At each selected age, one pellet was finely ground, and approximately 20–30 mg of powder was placed into pre-tared alumina crucibles. Thermogravimetric analysis was carried out under a pure argon atmosphere, with a constant gas flow of 20 mL/min. Samples were heated from 22 °C to 1000 °C at a constant heating rate of 10 °C/min.

The mass loss occurring in the temperature range of 390–540 °C was attributed to the dehydroxylation of calcium hydroxide (CH) and was used to estimate the CH content of the pastes. Occasional duplicate tests were performed to verify the repeatability of the measurements.

The CH content was calculated following the stoichiometric approach proposed by Córdoba et al. [31], using the molecular mass ratio between calcium hydroxide and the water released during dehydroxylation:

$$\mathrm{CH} = w_{\mathrm{L,CH}} \frac{M_{\mathrm{CH}}}{M_{\mathrm{H_2O}}} \tag{2.4.4}$$

where CH is the calcium hydroxide content expressed as mass percentage (wt.%), $w_{\mathrm{L,CH}}$ is the mass loss associated with CH dehydroxylation in the 390–540 °C interval, $M_{\mathrm{CH}} = 74$ g/mol is the molar mass of $Ca(OH)_2$, and $M_{\mathrm{H_2O}} = 18$ g/mol is the molar mass of water.

Results

3.1 Compressive Strength

Figure 3.1 presents the compressive strength development of all mixtures as a function of curing age (Figure 3.1A). The incorporation of CSFT resulted in a dual response governed by both curing age and replacement level. All CSFT-modified mixtures exhibited reduced early-age compressive strength (2–14 days) compared to the OPC mixture. This reduction is consistent with clinker dilution effects and the limited early-age reactivity typically observed in cementitious systems incorporating supplementary materials, which delays the formation of load-bearing hydration products at early ages [2, 4, 14]. The most pronounced reduction was observed for CSFT-30 (black dash-dotted line), with strength losses of approximately 35% at 14 days, whereas CSFT-05 (red solid line) exhibited average strength differences of about 6% relative to the OPC mixture over the 2–14 day period, indicating that low replacement levels exert a limited influence on early-age strength.

Figure 3.1B summarizes the compressive strength at 28 days. Low–CSFT–replacement–levels ($\leq$10%) mixtures achieved strengths comparable to the OPC mixture, whereas mixtures with higher replacement levels led to a progressive reduction in compressive strength. This reduction at increasing CSFT contents reflects the balance between clinker dilution and the limited contribution of supplementary materials at the standard design age of 28 days, for which mechanical performance is still dominated by clinker content [2, 4, 14].

At curing ages beyond 56 days, the strength gap between OPC and CSFT-modified mixtures progressively decreased. The individual results of the compressive strength of CSFT-05 and CSFT-10 approached, and in some cases matched, the compressive strength of the OPC mixture by 90–180 days. This progressive reduction in the strength gap at extended curing ages is clearly illustrated by the compressive strength values at 180 days shown in Figure 3.1C. The observed strength recovery is consistent with continued hydration kinetics, whereby early clinker dilution is gradually compensated by microstructural densification at extended curing ages [4, 15]. In addition, the fine particle size of CSFT ($<$60 µm) may enhance physical packing effects, contributing to reduced porosity and supporting the development of load-bearing C–S–H at extended curing ages [2, 12–14]

Mixtures with higher replacement levels (CSFT-20 and CSFT-30) maintained lower average strength values throughout the curing period of this work; however, both exhibited clear upward trends beyond 56 days. Although the reduced clinker content of the mixtures constrains ultimate strength development, particularly at high replacement levels where clinker-driven hydration dominates early-age performance [2, 4], a sustained strength increase was observed at later curing ages. The sustained strength development at later curing ages suggests that CSFT may contain slowly reacting phases or promote delayed hydration-related processes (like create spaces to accomodate hydration products) that progressively contribute to strength development [14, 15].

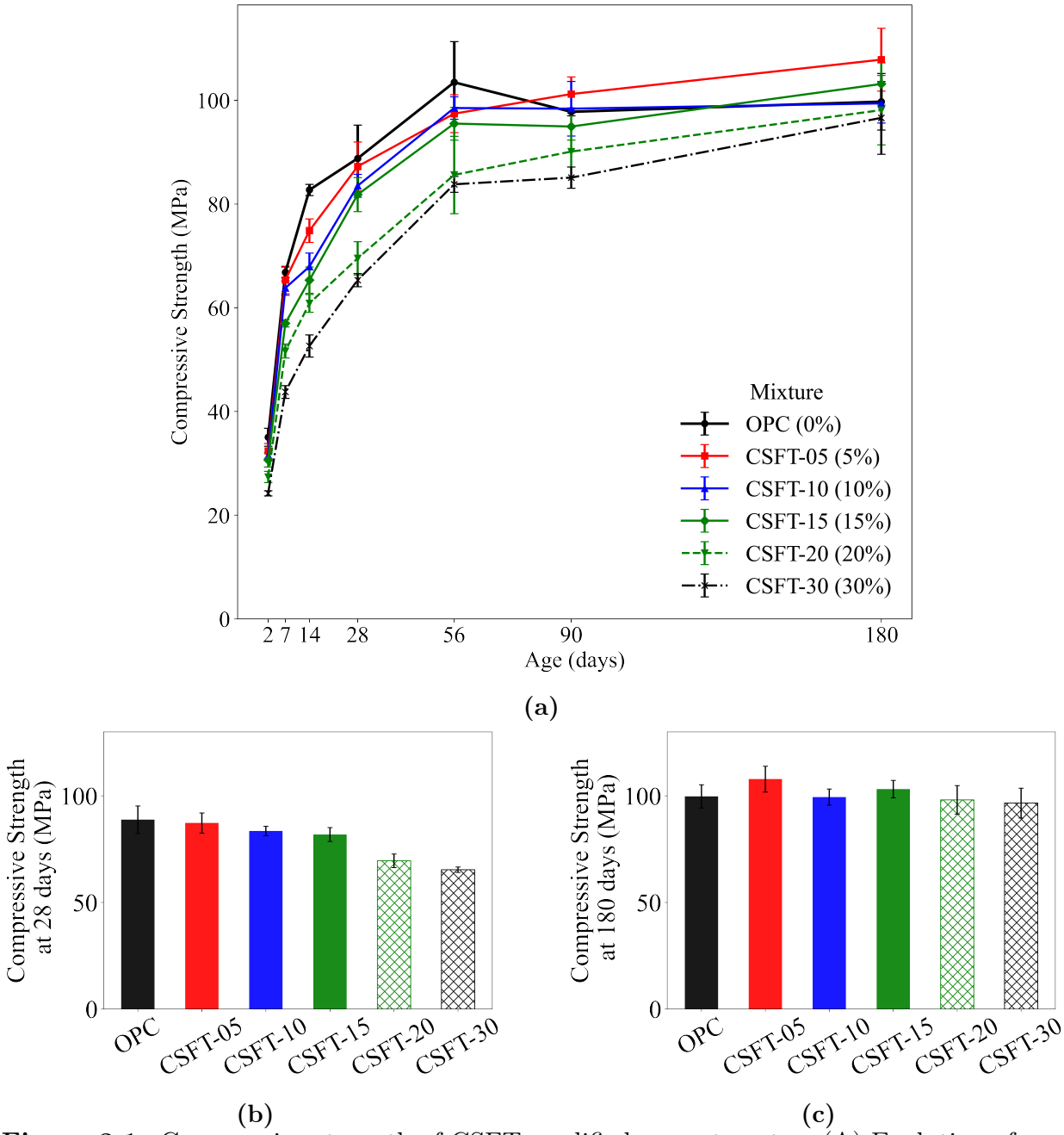

Figure 3.1. Compressive strength of CSFT-modified cement pastes. (A) Evolution of compressive strength as a function of curing age for OPC (black solid line with circular markers), CSFT-05 (red solid line with square markers), CSFT-10 (blue solid line with triangular markers), CSFT-15 (green solid line with diamond markers), CSFT-20 (green dashed line with triangular markers), and CSFT-30 (black dash-dotted line with cross markers). (B) Compressive strength at 28 days for all mixtures, where solid-colored bars represent OPC and low to moderate CSFT replacement levels ($\leq$15%), while hatched bars indicate higher replacement levels (20% and 30%). (C) Compressive strength at 180 days, presented using the same color and pattern coding as in (B). Error bars represent one standard deviation. Overall, the results show a reduction in compressive strength at early ages with increasing CSFT content, while differences between mixtures tend to decrease at later curing ages, particularly for low to moderate replacement levels.

Figure 3.2 shows the linear dependence of compressive strength on CSFT replacement level for each mixture at different curing ages. The negative slopes of the linear adjustment observed at early ages (2–28 days) indicate a strong sensitivity of early compressive strength to clinker dilution, reflecting the dominant role of clinker-driven hydration during the initial stages in systems incorporating supplementary materials [2, 4]. As age evolves, the magnitude of the slope progressively decreases, indicating a reduced dependence of compressive strength of the mixtures on CSFT content at later ages. This behavior is associated with the progressive development of the cementitious matrix and the diminishing influence of replacement level on strength as hydration advances [4, 14].

At 180 days, the -0.21 slope indicates that long-term compressive strength becomes increasingly insensitive to replacement level. This attenuation of strength sensitivity reflects the reduced influence of clinker content on mechanical performance at extended curing ages, as hydration and microstructural refinement continue beyond early-age stages in systems containing low-reactivity supplementary materials [4, 12, 15]. From a performance-based perspective, this trend suggests that defining design strength at later ages may enable higher levels of OPC replacement by materials such as CSFT without proportionally penalizing long-term mechanical performance, in line with frameworks proposed for low-clinker cementitious systems [2, 12, 14].

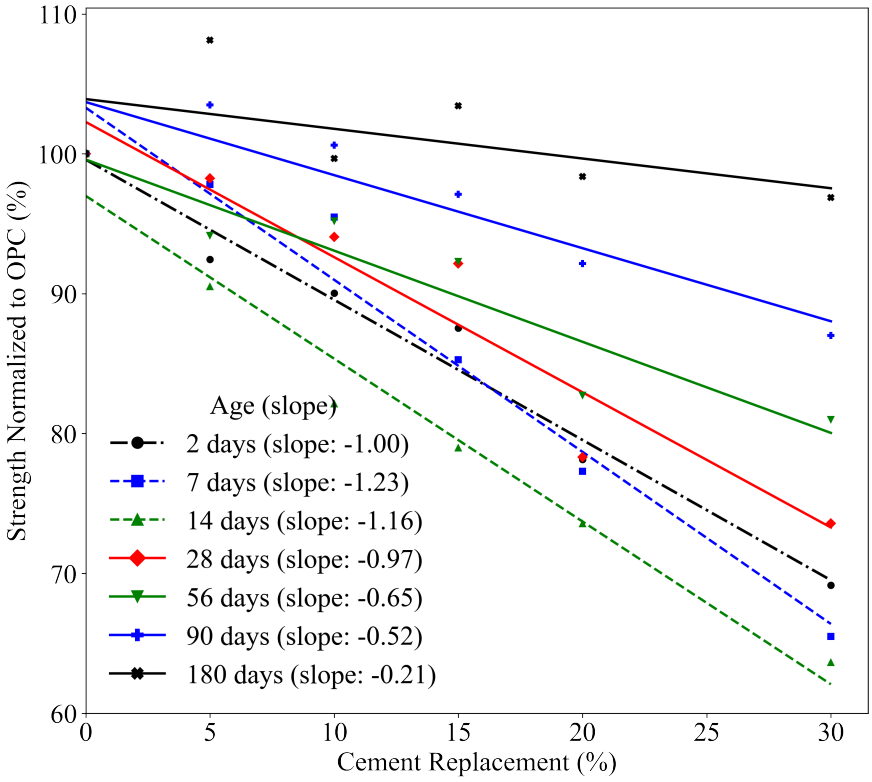

Figure 3.2. Linear trends of compressive strength as a function of CSFT replacement level at different curing ages. Symbols represent experimental compressive strength values, while solid and dashed lines correspond to linear regressions fitted for each curing age. Curves are shown for 2 days (black dash-dotted line with circular markers), 7 days (blue dashed line with square markers), 14 days (green dashed line with triangular markers), 28 days (red solid line with diamond markers), 56 days (green solid line with inverted triangular markers), 90 days (blue solid line with plus markers), and 180 days (black solid line with cross markers). The progressive reduction in the absolute value of the slope with increasing curing age indicates a decreasing sensitivity of compressive strength to CSFT replacement level at later ages.

3.2 Flexural Strength

Flexural strength results (Figure 3.3) exhibited high variability across all CSFT replacement levels, without a consistent or monotonic trend with curing age or CSFT content. The pronounced scatter prevents the identification of a clear relationship between flexural strength and mixture composition. This behavior reflects the inherently brittle response of unreinforced cement paste specimens, whose flexural performance is governed by fracture processes that are highly sensitive to surface defects, microcracks, and microstructural heterogeneities [32–34]. In dense, low water-to-binder ratio matrices such as those employed in this study (w/b = 0.30), localized defects and early-age microcracks can trigger premature cracking under flexural loading, thereby limiting the reliability of flexural strength as a standalone

indicator of mechanical performance [12, 33–35]. Recent experimental and analytical studies have shown that even nanometric or sub-millimetric shrinkage-induced microcracks can significantly reduce the apparent flexural strength while having a limited impact on compressive strength [33, 35]. This explains why the highest variability was observed at early curing ages (2–14 days), even though compressive strength displayed more consistent and interpretable trends over the same period. This discrepancy between the highly scattered flexural strength results and the more consistent compressive strength trends has been documented in cementitious systems prone to autogenous and drying shrinkage, where restrained volumetric deformations generate internal stresses that may lead to microcracking prior to mechanical testing [33, 34]. Such pre-existing defects are not uniformly distributed throughout the material, resulting in unpredictable fracture paths and amplified scatter in flexural strength measurements, particularly in paste-scale specimens where stress redistribution mechanisms are limited [32, 35].

Autogenous shrinkage, driven by self-desiccation in low water-to-binder ratio cement pastes, becomes significant during early hydration and may locally exceed the tensile capacity of the material [33, 34, 36]. The interaction of chemical and autogenous shrinkage mechanisms promotes the early formation of microcracks that strongly govern tensile-related performance, as demonstrated by recent crack-quantification approaches based on advanced image analysis and machine learning techniques [35].

Despite this inherent variability, some qualitative tendencies emerged at later ages. By 180 days, CSFT-05 and CSFT-10 exhibited flexural strength values comparable to OPC, suggesting progressive microstructural refinement and improved stress redistribution as hydration advances [14]. This late-age flexural response is consistent with the compressive strength evolution previously discussed for low CSFT replacement levels. In contrast, CSFT-30 consistently showed the lowest flexural strength across all curing ages. The unstable response of the tensile strength of the low w/c mixtures presented in this work reflects the dominant role of defect-related cracking in dense cementitious systems incorporating high levels of low-reactivity or filler-type materials, where tensile performance is governed primarily by brittle behaviour of the mixtures [32–34].

The flexural strength results illustrate the limitations of flexural strength testing when applied to isolated cement pastes, particularly in low w/c mixtures, for which fracture behavior is governed by localized defects rather than by bulk matrix properties. Under these conditions, complementary indicators such as ultrasonic pulse velocity and electrical resistivity provide more robust insight into mechanical behavior and microstructural development in CSFT-modified systems, as emphasized in multi-parameter assessment approaches for low-reactivity and filler-dominated SCMs [14, 34].

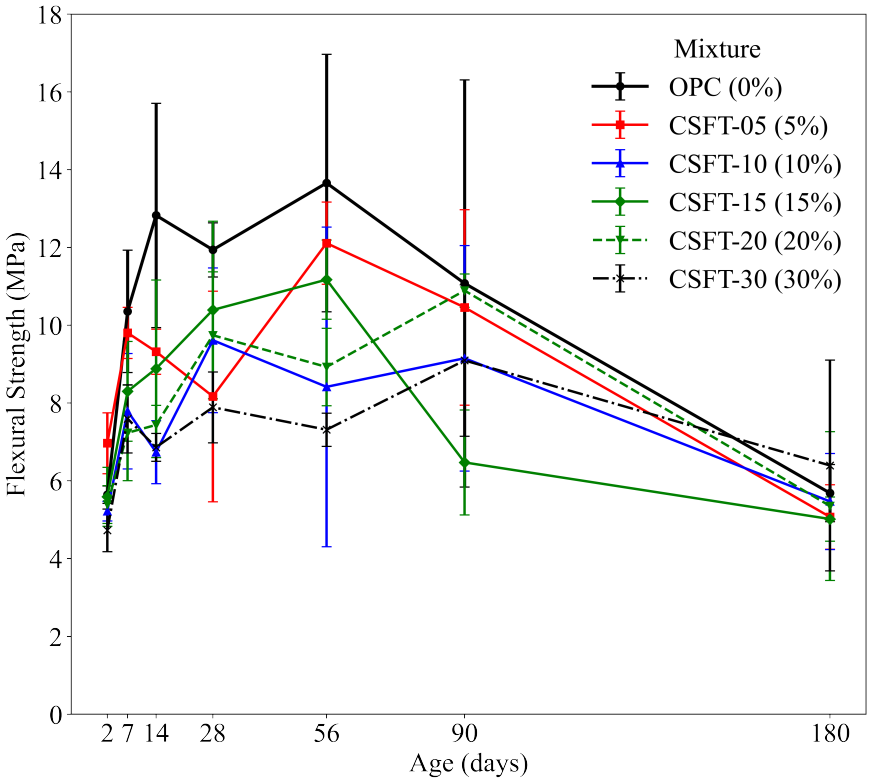

Figure 3.3. Flexural strength of CSFT-modified cement pastes as a function of curing age. Results are shown for OPC (black solid line with circular markers), CSFT-05 (red solid line with square markers), CSFT-10 (blue solid line with triangular markers), CSFT-15 (green solid line with diamond markers), CSFT-20 (green dashed line with triangular markers), and CSFT-30 (black dash-dotted line with cross markers). Error bars represent one standard deviation. The flexural strength results exhibit substantial scatter across all mixtures and curing ages, with no systematic dependence on CSFT replacement level or a consistent evolution with curing time.

3.3 Electrical Resistivity

Figure 3.4 shows the evolution of surface electrical resistivity for all mixtures as a function of curing age. At early ages (2–7 days), resistivity values of the mixtures decreased systematically with increasing CSFT replacement. Mixtures with higher CSFT contents, particularly CSFT-20 (green dashed line) and CSFT-30 (black dash-dotted line), exhibited the lowest average resistivity values, reflecting higher ionic mobility and a less connected solid skeleton at early ages as a result of reduced clinker content and delayed hydration [2, 33]. The latter behavior is consistent with the reduced early-age mechanical performance and delayed development of hydration products observed in compressive strength results of cement pastes incorporating CSFT as partial OPC replacement[4, 15].

From 28 days onward, resistivity increased markedly for all mixtures, indicating pro-

gressive microstructural densification and reduced pore connectivity [33]. Low replacement mixtures, especially CSFT-05 (red solid line) and CSFT-10 (blue solid line), exhibited a rapid increase in resistivity and reached values comparable to the OPC mixture by 90–180 days. This convergence suggests that the incorporation of limited amounts of CSFT does not hinder long-term pore refinement and may benefit from physical filler effects and continued hydration, which contribute to the progressive reduction of ionic transport pathways [4, 12–14].

Although CSFT-20 and CSFT-30 maintained lower absolute resistivity values throughout the curing period in this work, their monotonic increase with age indicates ongoing microstructural densification and gradual improvement of the solid-phase network [4]. The parallel upward trends observed for all mixtures indicate that CSFT primarily delays early microstructural development rather than inhibiting long-term refinement, reflecting hydration processes that progressively reduce pore connectivity despite clinker dilution [2, 14]. These resistivity trends therefore indicate that CSFT modifies early-age transport properties while still allowing progressive microstructural improvement at extended curing ages.

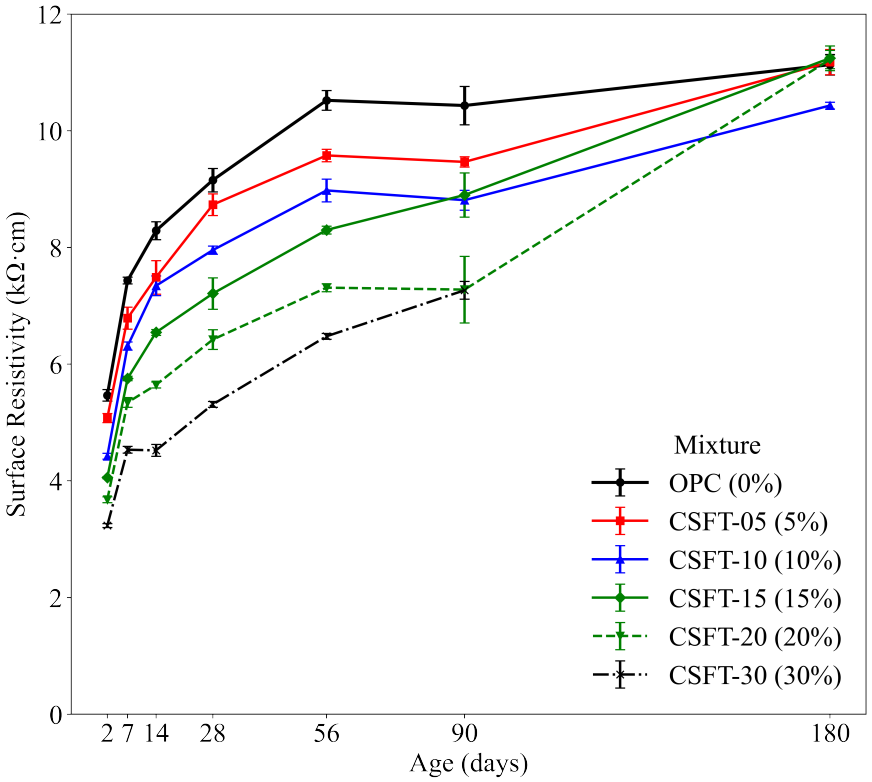

Figure 3.4. Evolution of surface electrical resistivity of CSFT-modified cement pastes as a function of curing age. Results are shown for OPC (black solid line with circular markers), CSFT-05 (red solid line with square markers), CSFT-10 (blue solid line with triangular markers), CSFT-15 (green solid line with diamond markers), CSFT-20 (green dashed line with triangular markers), and CSFT-30 (black dash-dotted line with cross markers). Error bars represent one standard deviation. Surface electrical resistivity increases with curing age for all mixtures, with lower values generally observed for higher CSFT replacement levels.

3.4 Ultrasonic Pulse Velocity (UPV)

Ultrasonic pulse velocity results (Figure 3.5) provide complementary information on matrix continuity, uniformity, and stiffness development. At early ages, UPV values of the mixtures decreased with increasing CSFT replacement, with CSFT-20 and CSFT-30 exhibiting the lowest average velocities. The latter behavior reflects a less stiff and less mature matrix resulting from reduced clinker content and delayed hydration, which limit the early formation of load-bearing hydration products and continuous solid phases [2, 4].

As curing progressed, UPV increased for all mixtures, indicating gradual stiffening and improved continuity of the cementitious matrix as hydration advanced [4]. Mixtures with low CSFT content, particularly CSFT-05 (red solid line) and CSFT-10 (blue solid line), showed pronounced UPV gains between 28 and 90 days and converged toward the average value of the OPC mixture by 180 days. This convergence indicates that limited CSFT incorporation does not compromise long-term matrix integrity, as the progressive development of hydration products and physical packing effects compensate for early-age dilution [2, 13, 14].

Higher replacement mixtures (CSFT-20 and CSFT-30) maintained lower UPV average values across all curing ages; however, their consistent upward trends indicate ongoing structural development rather than stagnation. This evolution reflects the gradual formation and densification of the solid phase under reduced clinker availability, characteristic of cementitious systems incorporating delayed-reactivity supplementary materials [4]. The absence of abrupt UPV reductions or irregular behavior further indicates that CSFT incorporation does not disrupt bulk matrix continuity, but instead results in a slower and more progressive stiffness development [2].

UPV and electrical resistivity results provide consistent evidence of delayed yet continuous microstructural development in CSFT-modified systems. These nondestructive indicators capture the evolution of internal connectivity and stiffness associated with hydration progress and pore refinement, complementing mechanical testing by revealing changes that precede or accompany strength development at extended curing ages [14, 15].

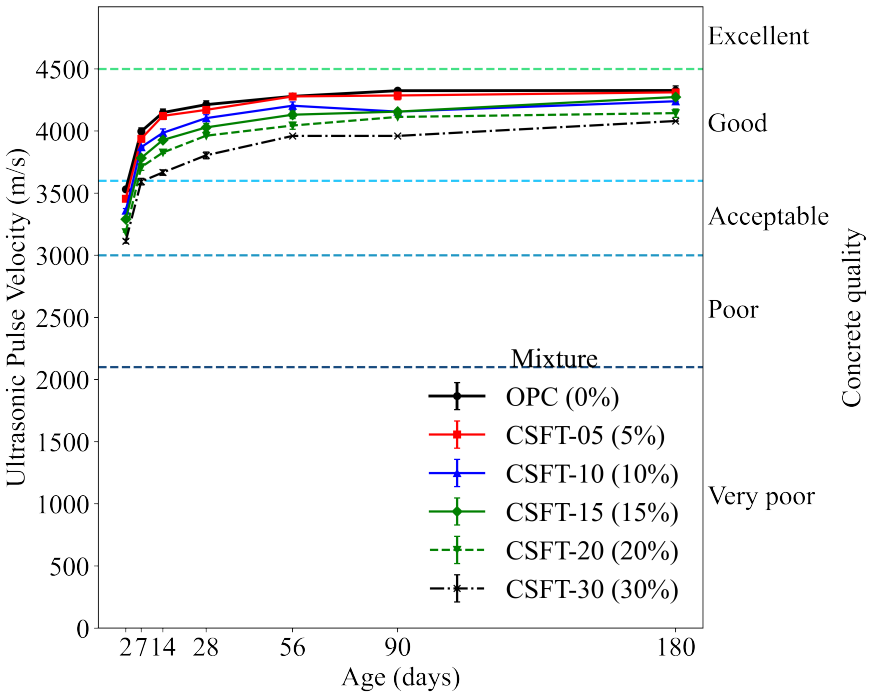

Figure 3.5. Evolution of ultrasonic pulse velocity (UPV) of CSFT-modified cement pastes as a function of curing age. Results are shown for OPC (black solid line with circular markers), CSFT-05 (red solid line with square markers), CSFT-10 (blue solid line with triangular markers), CSFT-15 (green solid line with diamond markers), CSFT-20 (green dashed line with triangular markers), and CSFT-30 (black dash-dotted line with cross markers). Error bars represent one standard deviation. The horizontal reference bands indicate qualitative concrete quality ranges based on ultrasonic pulse velocity, as commonly reported in the literature [37]. These bands are included for visual guidance only; although such classifications are defined for concrete rather than cement pastes, they are used here to provide a qualitative indication of paste uniformity and to highlight the limited influence of CSFT replacement on UPV development.

3.5 Thermogravimetric Analysis (TGA)

Figures 3.6 and 3.7 present the evolution of mass loss associated with the dehydration of C–S–H and chemically bound water in the 125–300 °C range, and the dehydroxylation of portlandite (CH) in the 390–540 °C range, respectively. These temperature intervals are commonly employed in thermogravimetric analyses of cementitious systems to track the formation and evolution of hydration products, as they correspond to the stability domains of bound water in C–S–H and calcium hydroxide [4, 38]. The results therefore provide insight into the relative development of hydration products as a function of curing age and CSFT replacement level.

The mass loss associated with C–S–H and chemically bound water (Figure 3.6) increased

progressively with curing age for all mixtures. At early ages, the OPC mixture exhibited the highest mass loss values, whereas CSFT-modified mixtures showed systematically lower values. The latter behavior is consistent with the reduction in early hydration expected from clinker dilution, as widely reported for cement systems incorporating supplementary cementitious materials with slow reaction kinetics [4, 15, 39].

As curing age progressed, the differences in C–S–H-related mass loss between the OPC mixture and CSFT mixtures gradually decreased across all replacement levels. From 56 to 90 days onward, and particularly at 180 days, the C–S–H-related mass loss values of the CSFT mixtures approached those of the OPC mixture. This recovery of C–S–H-related bound water with time mirrors the long-term compressive strength development reported in Section 3.1 and is consistent with observations reported for blended cement systems incorporating fly ash or slag, where delayed hydration or pozzolanic reactions contribute to C–S–H formation at later ages [4, 39].

In contrast, the CH content estimated from mass loss in the 390–540 °C range (Figure 3.7) exhibited a systematically different trend. For all curing ages, CH content decreased monotonically with increasing CSFT replacement level, and no significant recovery with time was observed for any of the CSFT mixtures. This sustained reduction in portlandite content is primarily attributed to clinker dilution and reflects the lower amount of calcium hydroxide generated by clinker hydration, a trend extensively documented for cementitious systems containing supplementary materials [4, 39].

The simultaneous observation of (i) a persistent reduction in CH content with increasing CSFT replacement level and (ii) a progressive recovery of the C–S–H content at later curing ages highlights the decoupled evolution of these two hydration products. Similar behavior has been reported by Salgiani et al. [39] for blended systems incorporating fly ash or slag, in which portlandite content decreases steadily with increasing replacement, while C–S–H content partially recovers at advanced ages due to delayed chemical contributions from the supplementary material. In the present study, this contrasting evolution suggests that, beyond clinker dilution effects, part of the available portlandite may be involved in delayed chemical reactions contributing to additional C–S–H formation. While this hypothesis cannot be confirmed solely on the basis of TGA results, it is consistent with the behavior reported for cementitious systems incorporating slowly reactive supplementary materials, where CH consumption and late-stage C–S–H development may occur concurrently [4, 39].

The TGA results indicate that CSFT-modified systems exhibit a hydration behavior characterized by a sustained reduction in portlandite content and a progressive recovery of C–S–H-related bound water at later ages. While these observations are compatible with a combined filler effect and a delayed chemical contribution from CSFT, the TGA data alone do not allow a quantitative assessment of its intrinsic reactivity or pozzolanicity. Further investigations using complementary techniques are required to clarify the extent and mechanisms of this potential chemical contribution.

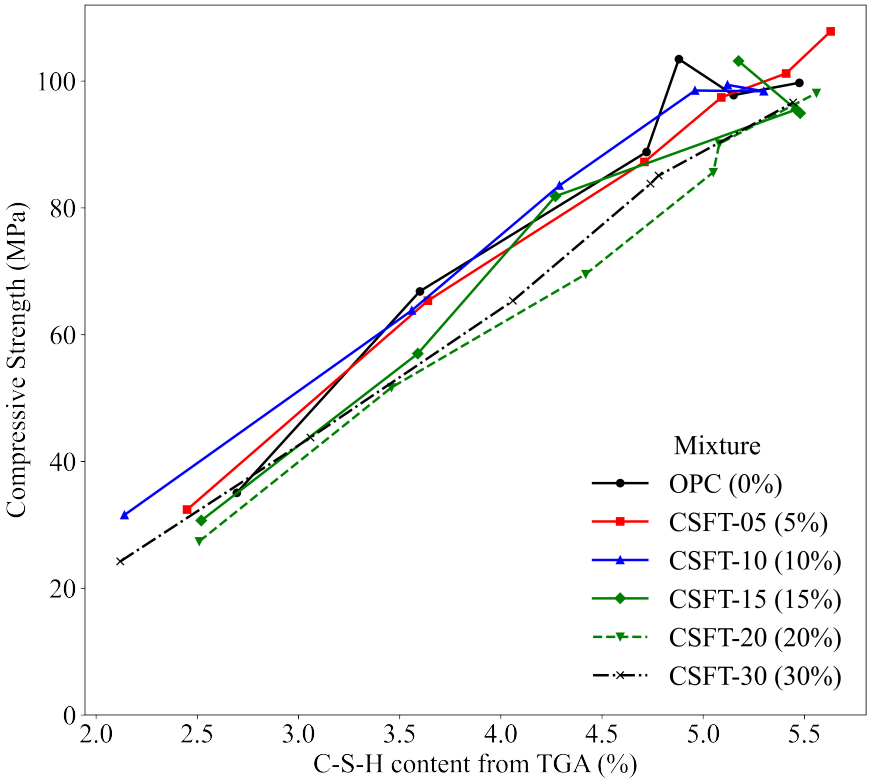

Figure 3.6. Relationship between C–S–H content, determined by thermogravimetric analysis, and compressive strength of CSFT-modified cement pastes at different curing ages. Results are shown for OPC (black solid line with circular markers), CSFT-05 (red solid line with square markers), CSFT-10 (blue solid line with triangular markers), CSFT-15 (green solid line with diamond markers), CSFT-20 (green dashed line with triangular markers), and CSFT-30 (black dash-dotted line with cross markers). Symbols represent experimental data, while connecting lines are included as visual guides. A linear relationship is observed between mass loss in this temperature interval and compressive strength, indicating that both parameters evolve in a similar manner with curing time across all mixtures.

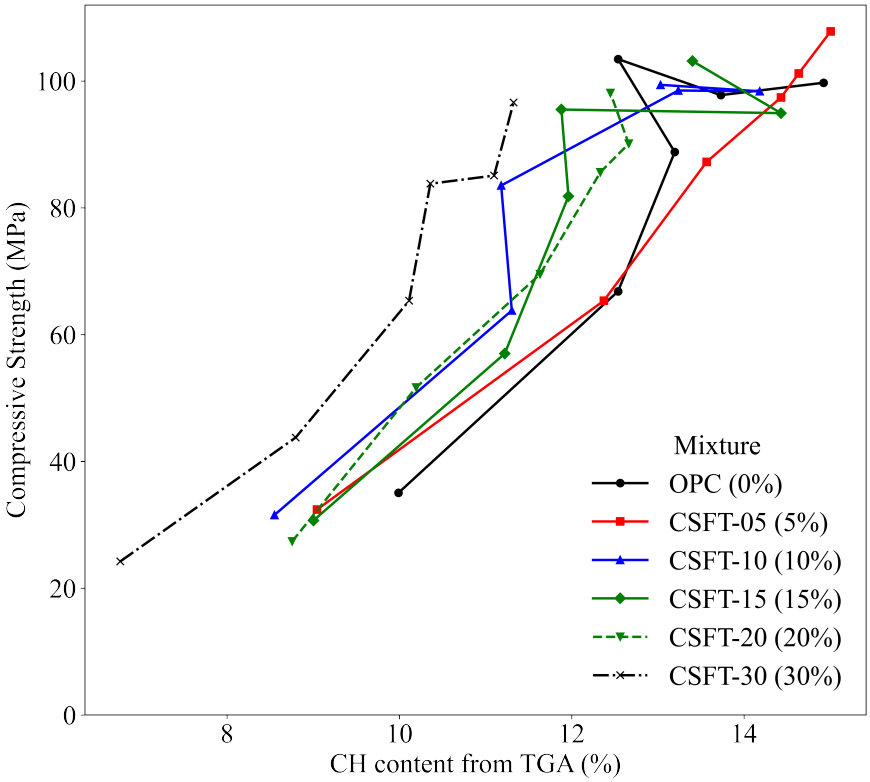

Figure 3.7. Calcium hydroxide (CH) content of CSFT-modified cement pastes as a function of curing age, estimated from thermogravimetric mass loss in the 390–540 °C temperature range. Results are shown for OPC (black solid line with circular markers), CSFT-05 (red solid line with square markers), CSFT-10 (blue solid line with triangular markers), CSFT-15 (green solid line with diamond markers), CSFT-20 (green dashed line with triangular markers), and CSFT-30 (black dash-dotted line with cross markers). CH content was calculated using Equation (1), and the selected temperature interval corresponds to portlandite dehydroxylation, as defined in the reference study from which the equation was adopted. In contrast to compressive strength, CH content does not exhibit a similar evolution with curing time, as CSFT-containing mixtures maintain a reduced CH content even at extended curing ages compared to OPC.

Discussion

The combined analysis of mechanical performance, nondestructive indicators, and thermogravimetric data reveals a consistent mechanistic framework governing the behavior of CSFT-modified cement pastes. Across all replacement levels, the incorporation of CSFT resulted in reduced early-age compressive strength, lower ultrasonic pulse velocity, and decreased electrical resistivity. These effects are primarily attributed to clinker dilution and the associated reduction in early hydration product formation,This is consistent with that reported in previous studies on cementitious systems incorporating materials with delayed hydration kinetics, such as those reported by Lothenbach et al. [4], Zunino et al. [14], and Suraneni et al. [15].

At extended curing ages, CSFT-containing systems exhibited progressive microstructural development. Compressive strength, electrical resistivity, and ultrasonic pulse velocity increased with curing time, with low–CSFT–replacement mixtures (CSFT-05 and CSFT-10) approaching or matching the performance of the OPC mixture by 90–180 days. Similar delayed convergence of mechanical and transport-related indicators has been reported for blended cement systems incorporating slowly reacting supplementary materials[4, 13, 15, 40]. In such systems, hydration is not suppressed but proceeds at a reduced rate over extended curing periods. In this context, early-age behavior is governed predominantly by clinker dilution effects, whereas delayed hydration processes or secondary reactions may contribute at later ages, becoming evident only beyond conventional performance assessment times [18, 41].

Thermogravimetric analysis provides additional insight into the hydration mechanisms associated with CSFT incorporation. The mass loss associated with C–S–H and chemically bound water in the 125–300 °C range increased with curing age for all mixtures and progressively converged across systems by 180 days. This evolution mirrors the long-term development of compressive strength and indicates that the formation of C–S–H is the primary driver of mechanical performance at advanced curing ages [2, 4, 39].

In contrast, the calcium hydroxide content estimated from mass loss in the 390–540 °C range remained consistently lower in CSFT-modified mixtures and decreased systematically with increasing replacement level. The CH evolution curves remained approximately parallel over time, indicating that portlandite content does not recover at later ages, even when C–S–H-related mass loss and compressive strength approach to the OPC mixture values. This sustained reduction in CH content is primarily associated with clinker dilution and the resulting lower availability of calcium hydroxide generated during hydration, a behavior widely documented for blended cement systems [4, 14, 39].

The simultaneous observation of a persistent reduction in CH content and a progressive recovery of C–S–H-related bound water at later ages highlights the decoupled evolution of these two hydration products. Similar behavior has been reported by Salgiani et al. [39], who showed that in systems incorporating fly ash or slag, portlandite content decreases steadily with increasing replacement level, while C–S–H content partially recovers at curing ages of 90 and 365 days due to delayed chemical contributions from the supplementary material. In the present study, this contrasting evolution suggests that, beyond purely physical filler effects, CSFT may contribute to hydration through delayed chemical reactions that promote additional C–S–H formation at curing ages of 90 and 180 days. While this interpretation cannot be confirmed solely on the basis of TGA results, it is consistent with hydration trends reported for cementitious systems incorporating slowly reactive supplementary materials, where CH consumption and late-stage C–S–H development may occur concurrently [4, 39].

Conclusions

This study investigated the mechanical performance, nondestructive indicators, and hydration behavior of cement pastes incorporating copper slag flotation tailings (CSFT) as a partial replacement of OPC, emphasizing the influence of curing age on performance evaluation. The results demonstrate that CSFT incorporation leads to a systematic reduction in early-age properties, including compressive strength, ultrasonic pulse velocity, and surface electrical resistivity. These early-age reductions are primarily associated with clinker dilution and the limited initial reactivity of CSFT, rather than with an inability of the system to develop a dense and mechanically competent microstructure at later ages.

At extended curing ages (90–180 days), mixtures with low to moderate CSFT replacement levels (5–10%) exhibited a progressive convergence in compressive strength and nondestructive indicators toward the OPC reference. This delayed convergence indicates that hydration and microstructural development in CSFT-modified systems proceed more slowly but continuously, and that performance assessed at conventional early ages does not fully capture their long-term behavior.

The findings indicate that CSFT behaves predominantly as a filler-dominated material with limited intrinsic reactivity, while potentially contributing to slow or delayed hydration-related processes at extended curing ages. The results also highlight the limitations of relying exclusively on 28-day compressive strength as a performance benchmark when assessing low-reactivity or filler-type supplementary materials. Extending the age used to define design performance may enable higher levels of clinker replacement without proportionally penalizing long-term mechanical behavior, thereby supporting the development of more sustainable cementitious systems.

The suitability of the conventional 28-day compressive strength benchmark is therefore challenged when evaluating cementitious systems incorporating low-reactivity or filler-dominated supplementary materials. For materials such as CSFT, assessments restricted to standard curing ages may underestimate long-term contributions that become evident only at extended curing periods, as reflected by the delayed convergence of mechanical performance and C–S–H development. Similar limitations of the 28-day criterion have been identified in both the scientific literature and technical reports addressing low-clinker cements and alternative SCMs, where extended curing ages are recommended to capture delayed hydration and progressive microstructural refinement processes [2, 41–44].

Bibliography

[1] Robbie M. Andrew. Global CO_2 emissions from cement production. *Earth System Science Data*, 10(1):195–217, 2018. doi: 10.5194/essd-10-195-2018.

[2] Karen L. Scrivener, Vanderley M. John, and Ellis M. Gartner. Eco-efficient cements: Potential economically viable solutions for a low-CO_2 cement-based materials industry. *Cement and Concrete Research*, 114:2–26, 2018. doi: 10.1016/j.cemconres.2018.03.015.

[3] Ministerio de Energía de Chile. Informe del sector cementero chileno 2023, 2023. Available online.

[4] Barbara Lothenbach, Karen Scrivener, and R. Douglas Hooton. Supplementary cementitious materials. *Cement and Concrete Research*, 41(12):1244–1256, 2011. doi: 10.1016/j.cemconres.2010.12.001.

[5] Zbigniew Giergiczny. Fly ash and slag. *Cement and Concrete Research*, 124:105826, 2019. doi: 10.1016/j.cemconres.2019.105826.

[6] F. Vargas and M. López. Development of a new supplementary cementitious material from the activation of copper tailings: Mechanical performance and analysis of factors. *Journal of Cleaner Production*, 182:427–436, 2018. doi: 10.1016/j.jclepro.2018.01.223.

[7] I. Alp, H. Deveci, H. Sungun, A. O. Yilmaz, A. Kesimal, and E. Yilmaz. Utilization of flotation wastes of copper slag as raw material in cement production. *Journal of Hazardous Materials*, 159(2–3):390–395, 2008. doi: 10.1016/j.jhazmat.2008.02.056.

[8] J. Esmaily and F. Aslani. Use of copper mine tailing in concrete: Strength characteristics and durability performance. *Journal of Materials in Civil Engineering*, 31(3):04019083, 2019. doi: 10.1061/(ASCE)MT.1943-5533.0002617.

[9] Jacob Ikotun, Rhoda Adeyeye, and Mike Otieno. Application of mine tailings sand as construction material – a review. *MATEC Web of Conferences*, 364:05008, 2022. doi: 10.1051/matecconf/202236405008.

[10] Deniz Adiguzel, Serkan Tuylu, and Hasan Eker. Utilization of tailings in concrete products: A review. *Construction and Building Materials*, 360:129574, 2022. doi: 10.1016/j.conbuildmat.2022.129574.

[11] Yipu Guo, Fulin Qu, and Wengui Li. Advancing circular economy and construction sustainability: transforming mine tailings into high-value cementitious and alkali-activated concrete. *npj Materials Sustainability*, 3(8), 2025. doi: 10.1038/s44296-025-00049-9.

[12] Viviana Bonavetti, H. Donza, G. Menéndez, O. Cabrera, and Edgardo Irassar. Limestone filler cement in low w/c concrete: A rational use of energy. *Cement and Concrete Research - CEM CONCR RES*, 33:865–871, 06 2003. doi: 10.1016/S0008-8846(02)01087-6.

[13] D. Bentz, Edgardo Irassar, B Bucher, and William Weiss. Limestone fillers conserve cement part 1: An analysis based on powers' model. *ACI Concrete International*, 31: 41–46, 01 2009.

[14] F. Zunino and M. López. Decoupling the physical and chemical effects of supplementary cementitious materials on strength and permeability: A multi-level approach. *Cement and Concrete Composites*, 65:19–28, 2016. doi: 10.1016/j.cemconcomp.2015.10.003.

[15] Prannoy Suraneni and Jason Weiss. Examining the pozzolanicity of supplementary cementitious materials using isothermal calorimetry and thermogravimetric analysis. *Cement and Concrete Composites*, 83:273–278, 2017. doi: 10.1016/j.cemconcomp.2017.09.007.

[16] Susan Bernal, Maria Juenger, Xinyuan Ke, Winnie Matthes, Barbara Lothenbach, Nele De Belie, and John Provis. Characterization of supplementary cementitious materials by thermal analysis. *Materials and Structures*, 50:1–13, 02 2017. doi: 10.1617/s11527-016-0909-2.

[17] P. Kumar Mehta. Rice husk ash – a unique supplementary cementing material. *Proceedings of the International Symposium on Advances in Concrete Technology*, pages 407–430, 1992.

[18] Almotasem Billah Ahmed. Assessing the effects of supplementary cementitious materials on concrete properties: a review. *Discover Civil Engineering*, 1(1):145, 2024. doi: 10.1007/s44290-024-00154-z.

[19] IDIEM. Official test report no. 1.396.487-0: Physical and mechanical characterization of portland cement. Technical report, Institute for Research, Development and Innovation of Structures and Materials (IDIEM), Universidad de Chile, Santiago, Chile, 2019.

[20] Nch2754: Residuos – procedimiento de lixiviación para determinar la característica de toxicidad, 2013. Basada en EPA Method 1311 (TCLP).

[21] Method 1311: Toxicity characteristic leaching procedure (tclp), 1992. Revision 0.

[22] L. D. Menéndez-Aguado, M. M. Sánchez, M. A. Rodríguez, A. L. C. Velázquez, and J. M. Menéndez-Aguado. Recycled mineral raw materials from quarry waste using hydrocyclones. *Materials*, 12(13):2047, 2019. doi: 10.3390/ma12132047.

[23] İ. Göktaş, O. Altun, N. A. Toprak, and D. Altun. Element based ball mill and hydrocyclone modelling for a copper ore grinding circuit. *Minerals Engineering*, 198:108090, 2023. doi: 10.1016/j.mineng.2023.108090.

[24] J. C. Cullivan, R. A. Williams, T. Dyakowski, and C. R. Cross. New understanding of a hydrocyclone flow field and separation mechanism from computational fluid dynamics. *Minerals Engineering*, 17(5):651–660, 2004. doi: 10.1016/j.mineng.2004.04.009.

[25] Z. Tang, L. Yu, F. Wang, N. Li, L. Chang, and N. Cui. Effect of particle size and shape on separation in a hydrocyclone. *Water*, 11(1):16, 2019. doi: 10.3390/w11010016.

[26] J. Wang, Y. Zheng, H. Wang, Z. Bai, and Y. Qiu. Investigation of the asymmetric flow structure in a hydrocyclone. *Asia-Pacific Journal of Chemical Engineering*, 19(4):e3080, 2024. doi: 10.1002/apj.3080.

[27] Standard test method for surface resistivity of concrete's ability to resist chloride ion penetration, 2019.

[28] Standard test method for pulse velocity through concrete, 2016.

[29] Standard test method for flexural strength of hydraulic-cement mortars, 2019.

[30] Standard test method for compressive strength of hydraulic-cement mortars (using portions of prisms broken in flexure), 2019.

[31] Gisela Cordoba, Ricarda Sposito, Mathias Köberl, Silvina Zito, Nancy Beuntner, Alejandra Tironi, Karl-Christian Thienel, and Edgardo F. Irassar. Chloride migration and long-term natural carbonation on concretes with calcined clays: A study of calcined clays in argentina. *Case Studies in Construction Materials*, 17:e01190, 2022. doi: 10.1016/j.cscm.2022.e01190.

[32] Arnon Bentur and Sidney Mindess. *Fibre Reinforced Cementitious Composites*. CRC Press, London, 2 edition, 2006. doi: 10.1201/9781482267747.

[33] Pietro Lura, Ole Mejlhede Jensen, and Jason Weiss. Cracking in cement paste induced by autogenous shrinkage. *Materials and Structures*, 42:1089–1099, 2009. doi: 10.1617/s11527-008-9445-z.

[34] Hassan Ghanem, Rawan Ramadan, Jamal Khatib, and Adel Elkordi. A review on chemical and autogenous shrinkage of cementitious systems. *Materials*, 17(2):283, 2024. doi: 10.3390/ma17020283.

[35] Xiaolan Zeng, Qian Deng, Shaohua Li, Hongbo Gao, and Qingliang Yu. Effects of autogenous shrinkage microcracks on UHPC: Insights from a machine learning based crack quantification approach. *Construction and Building Materials*, 428:136400, 2024. doi: 10.1016/j.conbuildmat.2024.136400.

[36] Erika Holt and Markku Leivo. Cracking risks associated with early age shrinkage. *Cement and Concrete Composites*, 26:521–530, 07 2004. doi: 10.1016/S0958-9465(03)00068-4.

[37] V. M. Malhotra and N. J. Carino. *Handbook on Nondestructive Testing of Concrete*. CRC Press, Boca Raton, FL, 2004.

[38] X. Feng, E.J. Garboczi, D.P. Bentz, P.E. Stutzman, and T.O. Mason. Estimation of the degree of hydration of blended cement pastes by a scanning electron microscope point-counting procedure. *Cement and Concrete Research*, 34(10):1787–1793, 2004. ISSN 0008-8846. doi: 10.1016/j.cemconres.2004.01.014.

[39] Mickaël Salgiani, Véronique Baroghel-Bouny, Matthieu Bertin, Sylvain Pradelle, and Julien Vincent. Phase assembly of cement pastes with scm at different ages. *Construction and Building Materials*, 224:144–157, 2019. ISSN 0950-0618. doi: 10.1016/j.conbuildmat.2019.07.059.

[40] Hoon Moon, Sivakumar Ramanathan, Prannoy Suraneni, Chang-Seon Shon, Chang-Joon Lee, and Chul-Woo Chung. Revisiting the effect of slag in reducing heat of hydration in concrete in comparison to other supplementary cementitious materials. *Materials*, 11(10), 2018. ISSN 1996-1944. doi: 10.3390/ma11101847.

[41] Ruben Snellings, Prannoy Suraneni, and Jørgen Skibsted. Future and emerging supplementary cementitious materials. *Cement and Concrete Research*, 171:107199, 09 2023. doi: 10.1016/j.cemconres.2023.107199.

[42] Ellis M. Gartner. Industrially interesting approaches to "low-CO_2" cements. *Cement and Concrete Research*, 34(9):1489–1498, 2004. doi: 10.1016/j.cemconres.2004.01.021.

[43] RILEM Technical Committee. Performance-based evaluation of supplementary cementitious materials. Technical Report TC 267-ISR, RILEM Publications, Paris, France, 2018.

[44] Federal Highway Administration. Reactivity of supplementary cementitious materials. Technical Report FHWA-HRT-25-050, U.S. Department of Transportation, Federal Highway Administration, Turner-Fairbank Highway Research Center, Washington, DC, 2025.